Received: 5 September 2021 | Revised: 10 October 2021 | Accepted: 11 October 2021

DOI: 10.1111/joa.13577

ORIGINAL PAPER

Journal of Anatomy ANATOMICAL SOCIETY WILEY

Río-Hortega's drawings revisited with fluorescent protein defines a cytoplasm-filled channel system of CNS myelin

Julia M. Edgar[1,2] | Eleanor McGowan[1] | Katie J. Chapple[1] | Wiebke Möbius[2,3] | Leandro Lemgruber[4] | Robert H. Insall[5] | Klaus-Armin Nave[2] | Anne Boullerne[6]

[1]Axo-Glial Group, Institute of Infection, Immunity and Inflammation, College of Medical, Veterinary and Life Sciences, University of Glasgow, Glasgow, UK

[2]Department of Neurogenetics, Max Planck Institute of Experimental Medicine, Göttingen, Germany

[3]Electron Microscopy Core Unit, Max Planck Institute of Experimental Medicine, Göttingen, Germany

[4]Glasgow Imaging Facility, Institute of Infection, Immunity and Inflammation, College of Medical, Veterinary and Life Sciences, University of Glasgow, Glasgow, UK

[5]Institute for Cancer Sciences, University of Glasgow, Glasgow, UK

[6]Department of Anesthesiology, University of Illinois at Chicago, Chicago, Illinois, USA

Correspondence
Julia M. Edgar, Axo-glial group, Institute of Infection, Immunity and Inflammation, College of Medical, Veterinary and Life Sciences, University of Glasgow, G12 8TA Glasgow, UK.
Email: Julia.Edgar@glasgow.ac.uk

Klaus-Armin Nave, Department of Neurogenetics, Max Planck Institute of Experimental Medicine, D-37075 Göttingen, Germany.
Email: Nave@em.mpg.de

Anne Boullerne, Department of Anesthesiology, University of Illinois at Chicago, Chicago, Illinois 60612, USA.
Email: abouller@uic.edu

Funding information
UK MS Society, Grant/Award Number: 38 and 127; NIH/National Library of Medicine, Grant/Award Number: G13LM011465; Deutsche Forschungsgemeinschaft, Grant/Award Number: TRR 274/1 2020—408885537; Research Center Nanoscale Microscopy and Molecular Physiology of the Brain; ERC Advanced Grants AxoGlia and MyeliNANO

Abstract

A century ago this year, Pío del Río-Hortega (1921) coined the term '*oligodendroglia*' for the 'interfascicular glia' with very few processes, launching an extensive discovery effort on his new cell type. One hundred years later, we review his original contributions to our understanding of the system of cytoplasmic channels within myelin in the context of what we observe today using light and electron microscopy of genetically encoded fluorescent reporters and immunostaining. We use the term *myelinic channel system* to describe the cytoplasm-delimited spaces associated with myelin; being the paranodal loops, inner and outer tongues, cytoplasm-filled spaces through compact myelin and further complex motifs associated to the sheath. Using a central nervous system myelinating cell culture model that contains all major neural cell types and produces compact myelin, we find that td-tomato fluorescent protein delineates the myelinic channel system in a manner reminiscent of the drawings of adult white matter by Río-Hortega, despite that he questioned whether some cytoplasmic figures he observed represented artefact. Together, these data lead us to propose a slightly revised model of the 'unrolled' sheath. Further, we show that the myelinic channel system, while relatively stable, can undergo subtle dynamic shape changes over days. Importantly, we capture an under-appreciated complexity of the myelinic channel system in mature myelin sheaths.

KEYWORDS
history, non-compact myelin, live-imaging, silver carbonate staining

[correction added on 15 Nov 2021, after first online publication: the email address for Anne Boullerne has been corrected]

1 | INTRODUCTION

The CNS myelinated fibre is the product of the intricate relationship between the neuron and the oligodendrocyte; one that is established by wrapping of the oligodendrocyte process around the axon through growth at the inner tongue (Snaidero et al., 2014). The complexity of the interaction is reflected in the morphology of the entwined cells, the molecular bridges that link them physically and functionally, especially at paranodal axo-glial connections (Lubetzki et al., 2020; Rasband & Peles, 2021), and in the correspondence between the physical dimensions of each (Bechler et al., 2018). Maintenance of the myelin sheath probably requires the continuous incorporation of new membrane at the inner tongue (Meschkat et al., 2020), and changes in neuronal activity can elicit changes in the thickness and length of individual sheaths, hypothesised to help fine-tune neuronal circuits (Arancibia-Cárcamo et al., 2017; Dutta et al., 2018; Yang et al., 2020). Thus, the myelin sheath is a dynamic structure that can be shaped and reshaped in response to signalling from the axon. The expanse of cytoplasmic channels that we refer to as the *myelinic channel system* likely serves as an infrastructure to enable dynamic shape changes of the myelin sheath, as a siphon for ions following action potential generation and a route for the transfer of cargoes for sheath maintenance, as well as to the glial–axonal junction for support of the axon.

Before Pío del Río-Hortega, the cytoplasmic channels within CNS myelin could not be visualised. The '*Schwann membrane'* (outer myelin cytoplasmic layer) nor the '*Mauthner membrane*' (myelin cytoplasmic periaxonal layer), both clearly visible in PNS without specific stain, could not be seen in the CNS and their presence was denied categorically in the 19th century (Boullerne, 2016). With the advent of a specific cytoplasm staining (Ehrlich method, methylene blue), Ramon y Cajal could reveal, after dissolution of myelin in preparation for resin inclusion, the Schwann membrane (cytoplasm) along the entire CNS internode as an extremely fine cuticle, especially visible at the nodes (Cajal, 1909–1911). However, Cajal believed the axon secreted myelin, and never succeeded in staining the processes of the oligodendrocyte; cells he dubbed '*apolar*' corpuscles or the CNS third element (Cajal, 1913). Río-Hortega was the first to stain the entire oligodendrocyte cytoplasm using a new silver carbonate staining, with which he also discovered microglia in the CNS (Río-Hortega, 1919). Subsequently, he focussed on the 1919 'interfascicular glia' with very few processes, for which he coined the term 'oligodendroglia' from Greek *oligo* [few] and *dendro* [branch] (Río-Hortega, 1921). Río-Hortega exclusively studied oligodendrocytes for 7 years afterwards and revealed in a comprehensive monograph, the intricacies, richness and diversity of cytoplasm associated with CNS white matter from cat and dog, but also rabbit, sheep, donkey, monkey, occasional post-mortem patients, and also grey matter across all CNS structures (Río-Hortega, 1928).

The refinement of electron microscopy (EM) in the 1960s led eventually to confirmation of the physical continuity between myelin and the oligodendrocyte (De Robertis et al., 1958), and the spiralling of CNS myelin around the axon across evolution (Metuzals and Maturana in frog; Uzman in chick and mouse; Peters and Hirano in rat, as reviewed in Bunge, 1968). The continuity between the oligodendrocyte and its myelin sheaths was elucidated again in the 1980s by light microscopy, with the focus shifting towards visualising the cytoplasm. Using dye filling of cells in optic nerve of young rats, Arthur Butt and Bruce Ransom described ' … cells [that] had 20–30 parallel processes approximately 50–200 μm in length …. connected to the cell body by thin processes … 15–30 μm [in length] …. Along their length the [longitudinal] processes intermittently appeared composed of two tightly intertwined processes, and often they ended in fine circular loops' (see Figures 1 and 3 in Butt & Ransom, 1989). These observations added a 3D perspective not easily afforded by EM. Nonetheless, the onerous task of manual 3D reconstruction by EM was conducted in feline and rat CNS, (Knobler et al., 1976; Remahl & Hildebrand, 1990); the confirming oligodendrocyte–axon configurations described by Río-Hortega; from his '*Schwannoid type*' one-to-one with the largest axons, to multiple small axons ensheathed by a single cell.

A further important 1980s development was the routine use of antibodies for immunostaining, helping elucidate molecular components of the myelinic channel system. 2′,3′-cyclic nucleotide 3′-phosphodiesterase (CNP), a lipid-anchored protein of 43 kDA, synthesised on free polysomes in the perinuclear area, was shown to occupy the cell soma, inner and outer tongues, paranodal loops and in large spinal cord fibres, also variable thin bands described as 'incisure-like membranes' (Trapp et al., 1988). Trapp's light microscopy and EM images of anti-CNP staining (see Figures 3A and 4C, Trapp et al., 1988) show bands akin to cytoplasmic channels buried deep inside compact myelin. A definitive CNS function of CNP has only recently been demonstrated, being to keep the cytoplasmic channels of myelin open (Snaidero et al., 2017). In the 21st century, the development and accessibility of relevant computing software facilitated 3D reconstruction of the myelinic channel system, first from confocal (Velumian et al., 2011) then EM (Snaidero et al., 2014). Coincidently, immunostaining, biochemistry and mass spectrometry methods identified other proteins of myelin-associated cytoplasm (myelinic channel system) including marker proteins such as Ermin (Brockschnieder et al., 2006) and ß-tubulin IV (Wu et al., 2009) as well as ubiquitous proteins of cytoplasm such as septins (Buser et al., 2009; Patzig et al., 2016) and Sirtuin 2 (Werner et al., 2007).

Nonetheless, in reports since Río-Hortega, the cytoplasm besides that of the well-established sheath edges (inner tongue, outer tongue and paranodal loops), the one buried deep into compact myelin, has been vastly overlooked and reported only incidentally (Bunge et al., 1961; Hildebrand et al., 1993; Hirano & Dembitzer, 1967). Schmidt-Lanterman incisures (SLIs), whose presence in CNS is restricted to the largest sheaths (Blakemore, 1969), contain the only generally acknowledged cytoplasm inside compact myelin notwithstanding that, in the CNS of higher vertebrates SLIs are extremely rare, often being undetected (Ghabriel & Allt, 1981). Indeed, we had to wait for molecular, genetic and advanced imaging approaches to demonstrate that cytoplasmic channels within compact myelin are important in myelin growth (myelinogenesis) (Snaidero et al., 2014),

and that once the sheath is mature, can provide access to Lucifer yellow (Velumian et al., 2011).

Notably, in contrast to the CNS, PNS myelin is ensheathed in a cuff of cytoplasm (see schematic Figure 1 in Peters, 1960) that traverses the entire internode. Furthermore, '*incisures of Schmidt-Lanterman*', described first in the 1870s, including by Ranvier (reviewed in Ghabriel & Allt, 1981) and later by others including Cajal (1909–1911), are frequent. SLIs are organised in series along the internode and provide the only route linking unequivocally outer tongue to inner tongue through a long helix of cytoplasm enclosed within myelin lamellae.

Together, these wealth of data highlight currently known functions, contents and morphology of the myelinic channel system. Here, in the centenary year that Río-Hortega coined the term 'oligodendroglia', we re-examine the myelinic channel system in relation to his drawings and descriptions.

2 | MATERIALS AND METHODS

2.1 | Mice

Transgenic mice were bred in the Biological Services Facility at the University of Glasgow, UK, under project licence PPL P78DD6 and the Animal Facility at the Max Planck Institute of Experimental Medicine in Göttingen, Germany, under project licence 33.9-42502-04-10/0288. Mice were housed in standard plastic cages with 1–5 littermates, with play tunnel, and were provided with food and water *ad libitum* and maintained in a 12-hour light–dark cycle. The ARRIVE guidelines are used as a framework for our studies in animal models, as described in detail in Bijland et al., 2019.

For PLP-CreERT2::'stop-floxed' CAG-td-tomato mice, male and female mice, which together harboured one copy of each of the two transgenes, were mated/time-mated to produce embryos/offspring harbouring combinations of tamoxifen-inducible PLP-CreERT2 (Leone et al., 2003; Weber et al., 2001) and/or the 'stop-floxed' Cre reporter gene CAG-td-tomato (Madisen et al., 2010).

When embryonic spinal cords were pooled to generate myelinating cell cultures, this led to sparse distribution of td-tomato fluorescent cells upon administration of 4-hydroxytamoxifen (4-HT) *in vitro*.

For immunoelectron microscopy, tamoxifen-induction of the td-tomato reporter was performed at the age of 8–9 weeks. Mice were injected intraperitoneally with 1 mg tamoxifen (100 µl of 10 mg/ml tamoxifen [Sigma-Aldrich, St. Louis, MO] in corn oil [Sigma-Aldrich]) for 5 consecutive days, followed by a 2-day break and 5 more days of injection as described previously (Leone et al., 2003).

For Cnp-Cre::'floxed-stop' CAG-td-tomato mice, *Cnp1*$^{+/Cre}$ mice (Lappe-Siefke et al., 2003) were crossed to mice hemizygous for the 'stop-floxed' CAG-td-tomato transgene (Madisen et al., 2010).

2.2 | Myelinating cell cultures

Pregnant female mice were killed at E13 by CO_2 overdose, followed by cervical dislocation. Spinal cords were extracted from the embryos, pooled and processed as described in Bijland et al. (2019) and cultured for up to 60 days. One micromole (final) 4-hydroxy tamoxifen was administered for 1 hour on day *in vitro* (DIV) 25 ± 5 days, after most myelin sheaths were mature.

2.3 | Immunocytochemistry

Myelinating cultures were fixed directly in 4% paraformaldehyde for 10 minutes at room temperature (RT), or by the addition of 1:1 v/v 8% paraformaldehyde at 37°C to cell culture media, then washed in PBS and permeabilised in methanol for 10 minutes at −20°C (Caspr1 and MBP) or 0.5% triton X for 10 minutes at room temperature (CNP, PLP and beta tubulin IV) and washed with PBS. Cultures were blocked for 1 hour with 10% goat serum in PBS or 1% BSA/10% goat serum/0.1% Tween-20 in PBS with 0.018 g/ml NaCl, at RT. Primary antibodies were rabbit anti-Caspr1(1:1000; kindly provided by Professor E Peles), rat anti-MBP (1:400, MCA409S; Bio-Rad), mouse anti-β tubulin 4 (1:200; ab11315; Abcam), rabbit anti PLP/DM20 (kindly gifted by Professor Nigel Groome) or mouse anti-CNP (1 in 400–800; ab6319; Abcam) diluted in blocking buffer and incubated overnight at 4°C. Bound antibodies were detected using Alexa 568, 488 or 647 goat anti-rabbit IgG, mouse IgG1 or rat IgG (1:1000; A21244; Thermo Fisher) by incubation for 1 hour at RT. Following careful washing in PBS and rinsing briefly in water, coverslips were mounted on glass slides in Mowiol containing DAPI (2 µg/ml).

2.4 | Microscopy including live imaging over multiple days

For live imaging, spinal cord cells were plated on custom made 35 mm diameter glass bottom Petri-dishes (Bijland et al., 2019) and maintained in a cell culture incubator at 37°C in humidified 5% CO_2 for up to 60 days *in vitro* (DIV). Live td-tomato rendered oligodendrocytes were imaged using an inverted Zeiss Observer Z1 SpinningDisc confocal microscope, equipped with a Yokogawa CSU-X1 filter wheel and spinning disc unit, a Photometrics Evolve 512 delta EM-CCD camera with 568 nm laser lines and a 63×/1.4 Oil Pln Apo objective and Zen imaging software. Alternatively, images were acquired with an inverted Zeiss Observer Z1 epi-fluorescence microscope equipped with an AxioCam MRc3, ×0.63 Camera Adaptor, ZEN 2012 blue edition software using a Zeiss plan-apochromat 63 × 1.4 oil objective. In both cases, cells were maintained at 37°C in a heated insert gassed with humidified 5% CO_2 and pH was checked during or after the experiment based on the colour of the phenol red-containing cell culture media. To study the dynamics of the myelinic channel, single focal planes or z-stacks (intervals indicated in figure legends) were taken over multiple days as described in figure legends.

High resolution images of immunostained myelinating cultures were taken using a Zeiss LSM 880 Confocal Microscope using a Zeiss Plan-Apochromat 63×/1.4 oil immersion objective and Zen Black software.

Images of CNP stained myelinating cultures (Figure 3) were taken using an inverted Olympus IX-70 wide-field epi-fluorescence microscope equipped with Image-Pro 6 image capture software. Cultures stained with antibodies to other epitopes, and tissue sections of *Cnp1*$^{+/Cre}$::'stop-floxed' CAG-td-tomato mice were imaged on a Zeiss Axioimager M2 upright epi-fluorescence microscope, equipped with a AxioCam MRm camera, a 63×/1.25 Oil Pln Neofluar objective and Zen imaging software.

2.5 | Super-resolution imaging

Structured Illumination microscopy (3D-SIM) was performed using a Zeiss Elyra PS.1 super-resolution microscope (Carl Zeiss, Germany). A plan-Apochromat 63×/1.4 Oil lens was used, and Z-steps of 0.2 μm were acquired (total thickness between 5 and 7 μm) in five rotations using the ZEN Black Edition Imaging software. For 3D modeling, acquired images were analyzed and processed by IMARIS software (Bitplane, Oxford Instruments).

2.6 | Immunoelectron microscopy

Immunoelectron microscopy of optic nerve was performed essentially as described in Weil et al. (2019). In brief, mice were perfused with a fixing solution composed of 0.25% glutaraldehyde, 4% formaldehyde, and 0.5% NaCl in phosphate buffer pH 7, according to Karlsson and Schultz (1965). Optic nerves were dissected and embedded in 10% gelatin for longitudinal or transverse sectioning. These blocks of gelatin-embedded nerves were infiltrated overnight in 2.3 M sucrose in 0.1 M phosphate buffer pH 7, mounted on aluminium pins and frozen in liquid nitrogen. Ultrathin cryosections were prepared using a diamond knife (cryoimmuno, 35°, Diatome, Biel Switzerland) and a UC6 ultramicrotome equipped for cryosectioning (Leica Microsystems, Vienna, Austria). Ultrathin sections were placed on hexagonal 100 mesh copper grids (Science Services, Munich, Germany) and labelled for td-tomato (polyclonal rabbit anti-RFP, Rockland, Limerick, USA) followed by incubation with protein A-gold (10 nm, Cell Microscopy Core, UMC Utrecht, The Netherlands). Images were taken with a LEO912 transmission electron microscope (Zeiss Microscopy GmbH, Oberkochen, Germany) using an on-axis 2k CCD camera (TRS, Moorenweis, Germany).

2.7 | Electron microscopy of myelinating cell cultures

This was carried out as described previously (Edgar et al., 2020; Thomson et al., 2006). Briefly, cultures were fixed in 2% paraformaldehyde/5% glutaraldehyde in 0.08 M sodium cacodylate buffer, pH 7.2, processed, sectioned and stained for electron microscopy and imaged using a JEOL JEM-100CX II electron microscope.

2.8 | 3D modelling and animation

Three-dimensional (3D) models and their animations were created using Blender v2.82. Reference images, being two-dimensional representations of z-stack microscopic data and historical figure 55 (Río-Hortega, 1928), were imported into the virtual scene during reconstruction to maximise veracity. For the microscopic models, the raw z-stack images were also consulted frequently during modelling. The myelinic channel system was created using Bezier curves of varying and tapered thickness. They were shaped proportionally to the reference images, and an emission shader was added to the mesh to enhance visualisation. Axons, extrapolated from the myelin data, were detailed with a noise texture and made transparent. Animations were created by adding an empty vector in the models' position and setting the camera and lighting to parent this vector. This allowed the vector to puppet the camera, thereby enabling the scene to be rendered at 24 frames per second while the vector rotated in 360 degrees and the camera captured the scene.

3 | RESULTS

3.1 | The forgotten drawings of Río-Hortega

Río-Hortega is best known for classifying myelinating oligodendrocytes in four types according to the axon diameter, orientation and number of internodes formed by a single cell. Forgotten is his extensive description of the cytoplasm associated to myelin across the entire axon diameter spectrum. In Supplementary File 1 we have curated quotes from his monograph (Río-Hortega, 1928), which illustrate his richly detailed observations of arborisation of processes connecting the cell body to myelin, and the complex patterning of myelin associated cytoplasm. Some of his drawings and our 3D interpretations of them are illustrated in Figure 1 and Supplementary movies 1B and C.

The semantic of myelin-associated cytoplasm is interesting because its presence was obvious, but its function not so, hence a quite diverse glossary has evolved since Río-Hortega, who himself called cytoplasm 'protoplasma', as customary for his time. Río-Hortega was aware that his new silver carbonate method stained the cytoplasm, leaving myelin invisible. The advent of EM revealed myelin's complex subcellular architecture. The outer and inner cytoplasm permanently lining longitudinally the internode (at the edge of compact myelin territory) has been termed *mesaxon*, *tongue*, *ridge*, *rim*, *loop or pocket*. The terms designating cytoplasm at the paranode were *terminal or paranodal loops or pockets*. These cytoplasmic regions were collectively designated *non-compact or uncompacted myelin*. Terms designating the less well-established cytoplasm coursing transversally (likely on the outer myelin wrap), or traversing deep into the compact

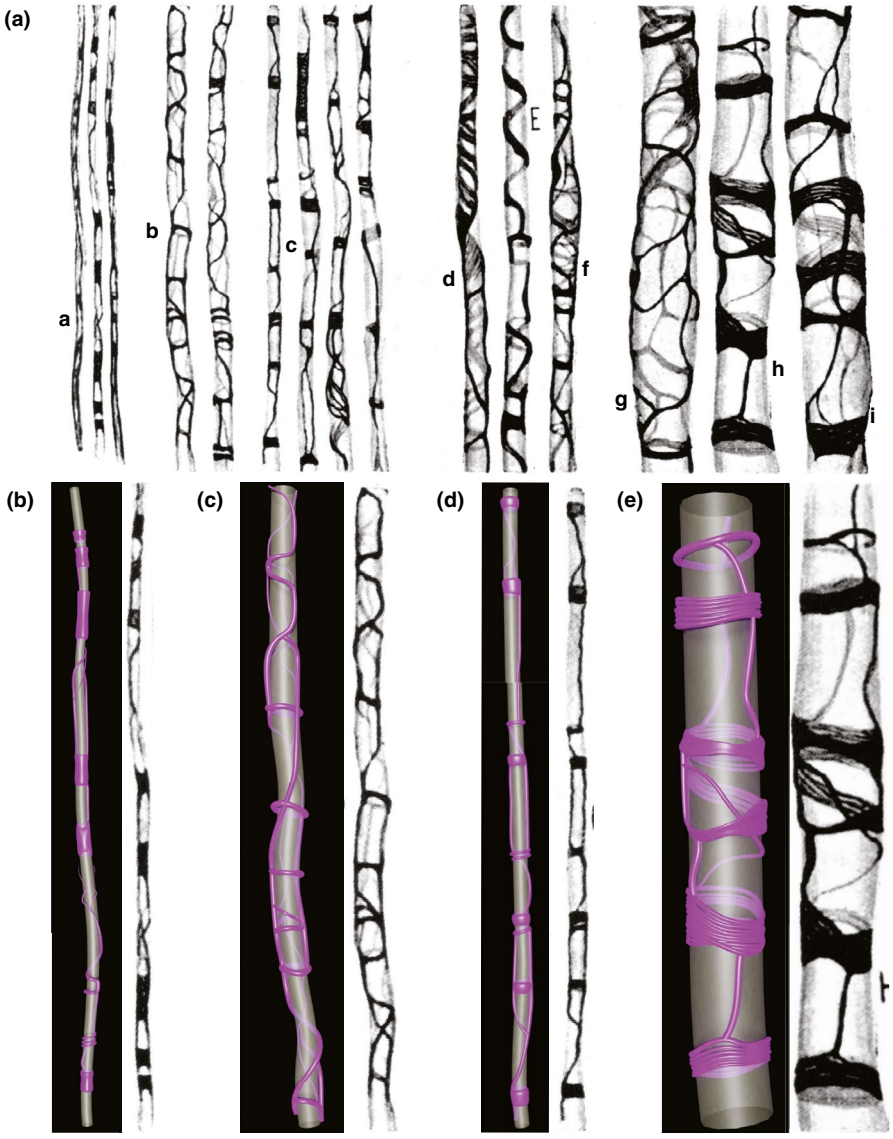

FIGURE 1 Panel (a) is reproduced from Figure 55, Río-Hortega, 1928, reporting different aspects of the perimyelinic sheaths formed by oligodendrocytes from thin (a) to medium thickness (b–f) to large (g–i) fibres. Río-Hortega (1928) described (a), subtle sheaths with little rings and plates; (b), fine reticula with turns of coil and rings; (c), rings of variable thickness connected by flanges; (d), laminar arrangement; (e), spiral arrangement; (f), reticular arrangement; (g), loose reticulum between two rings; (h), dense and laminar rings with fibrillar structure joined by trabeculae; (i) membranous funnel (likely a Schmidt-Lanterman incisure, see Supplementary file 1). Panels (b–e) show our 3D interpretations of Río-Hortega's (1928) drawings, across the entire axon diameter spectrum. The axolemma, encompassing the axon cylinder, is depicted in grey; cytoplasm of myelin in purple. In (e), we have interpreted some of the horizontal structures as being composed of multiple fine strands of cytoplasm but we cannot exclude that these are larger single structures. See also Supplementary movies 1B and C

layers, are more elusive: *pocket*, *cleft*, *incisure*, not to be confused with the proper Schmidt-Lanterman incisure in the PNS, called interchangeably *funnels* or *infundibulum* by Cajal and Río-Hortega. The first description of a *tubular reticulum* was for the inner tongue of medium sized sheaths in toad (Stensaas & Stensaas, 1968). More recently, the terms *cytoplasmic domains* (Trapp et al., 1987), *network of cytoplasmic interconnections* (Berry et al., 1995), *cytoplasmic network* (Velumian et al., 2011), *cytoplasmic compartments* (Butt, 2013), or *cytoplasmic channel* (Aggarwal et al., 2011; Snaidero et al., 2014; Weruaga-Prieto et al., 1996), have been used. Thus, we propose the term *myelinic channel system* to include the inner and outer tongue processes and paranodal loops, as well as cytoplasm-filled spaces associated with compact myelin itself.

3.2 | Soluble fluorescent proteins illuminate the myelinic channel

Río-Hortega questioned whether some of the cytoplasmic figures he observed represented artefact. To address this, we took advantage of transgenic mice expressing a cell-type specific fluorescent reporter expressed under the CAG promoter that diffuses through

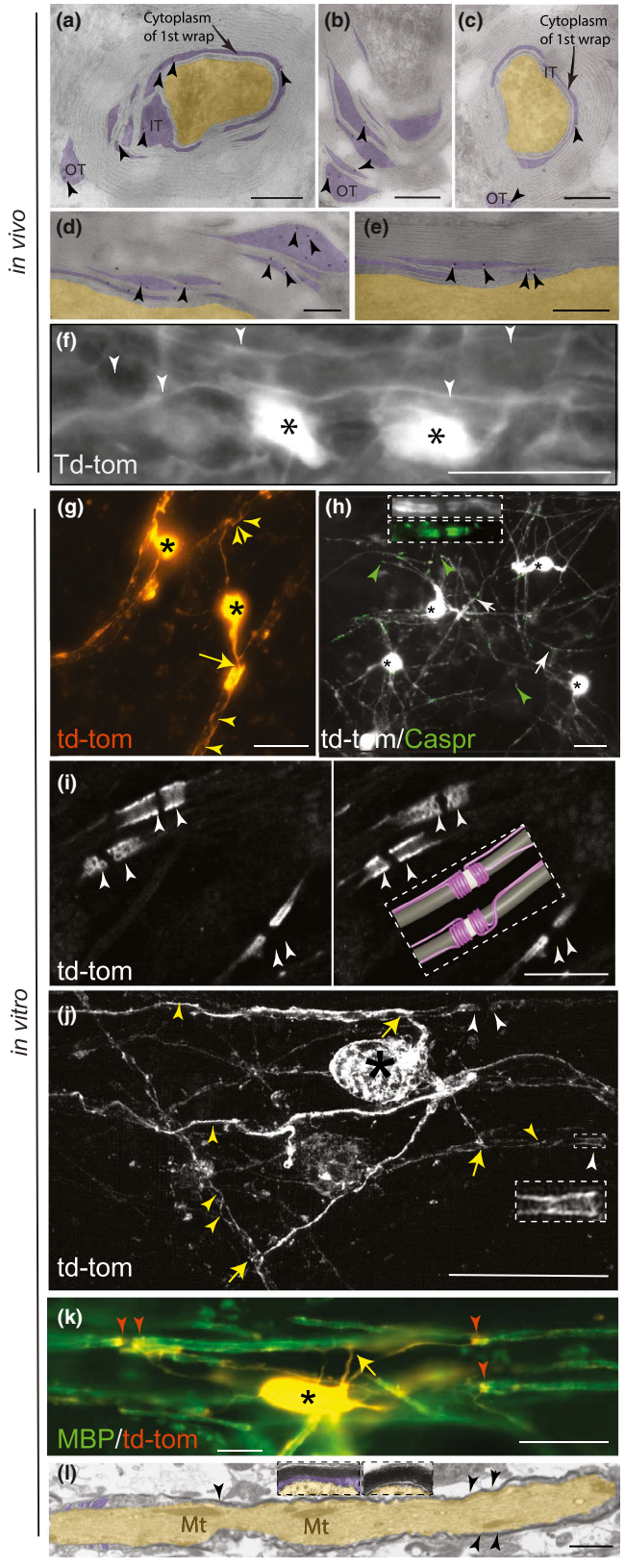

FIGURE 2 Td-tomato fluorescent protein delineates the myelinic channel system *in vivo* (part 1). Transverse (a–c) and longitudinal (d–e) sections of adult murine myelinated optic nerve fibres. (a–e) Immunoelectron microscopy showing localisation of antibody to td-tomato (10 nm gold particles, indicated by arrowheads) in cytoplasm-containing regions (purple overlay) of the myelin sheath including the inner tongue (IT), outer tongue (OT), between layers of the 1st wrap (arrows), and between layers of compact myelin. The axon is overlaid in yellow. Bars: 200 nm. (f) Epi-fluorescence microscopy of td-tomato rendered oligodendrocytes (asterisks) in adult murine spinal cord longitudinal section, showing myelin sheaths (white arrowheads) running in parallel. Bar: 20 μm. Td-tomato fluorescent protein delineates the myelinic channel system *in vitro* (part 2). (g) Epi-fluorescence microscopy live imaging of td-tomato rendered myelinating oligodendrocytes *in vitro*. Two cell bodies (asterisks) can be observed forming myelin sheaths. The yellow arrow points to the point of contact between a major process and the myelin sheath while the white arrow heads highlight coils of td-tomato rendered cytoplasm. Bar: 20 μm. (h) Epi-fluorescence microscopy images of td-tomato rendered oligodendrocytes (asterisks mark the cell bodies) in which Caspr1 stained paranodes (green; arrowheads) coincide with termini of myelin sheaths. Occasionally, in these sparsely labelled cultures, adjacent td-tomato positive sheaths form a node of Ranvier (white arrows and Supplementary Figure 2). Inset shows a higher magnification view of a node of Ranvier from a different field of view. (i) Two consecutive z-steps, 0.32 μm apart, captured using a confocal microscope illustrate td-tomato labelling of paranodes on two large diameter fibres and one smaller fibre. An idealised model, inferred from viewing the entire z-stack (Supplementary movie 2I) is provided for context. The internodal axon is depicted in grey, the node of Ranvier in white and the loops and inner and outer tongues in magenta. Bar: 10 μm. (j) Maximum intensity projection of a super-resolution z-stack (0.2 μm steps) of a td-tomato rendered cell, showing the paranodal loops at higher resolution (white arrowheads and inset). The yellow arrows point to the point of contact between a process and its myelin sheath while the yellow arrowheads highlight coils of td-tomato rendered cytoplasm. Bar: 20 μm. These details can be observed also in Supplementary movies 2J (1 and 2). (k) Epi-fluorescence microscopy captured image of MBP (green), which labels compact myelin. The cell body (asterisk), processes (one of which is indicated by the yellow arrow) and paranodes (red arrowheads) are td-tomato positive and MBP negative. Bar: 20 μm. (l) Electron micrograph of a longitudinal section of a myelinated axon demonstrating that compact myelin (arrowheads) forms in this *in vitro* model. Paranodal loops can be observed on the left of the image. Insets show higher magnification views of transverse sections of myelinated fibres. Cytoplasm-containing regions of myelin overlaid in purple, axon overlaid in yellow. Axonal mitochondria (Mt) are indicated. Bar: 250 nm

the cytoplasm to its furthermost reaches. Td-tomato fluorescent protein (Shaner et al., 2004) is a bright and stable fluorophore that does not bleach easily. To confirm that cytoplasm of myelin is fully rendered, we used immunoelectron microscopy to visualise the localisation of td-tomato at the ultrastructural level in optic nerve of adult PLPCreERT2::floxed stop td-tomato mice. We detected antibody to td-tomato (visible as 10 nm gold particles) in inner and outer tongues of myelin (Figure 2a–c), in the cytoplasm-filled space between the layers of the first myelin wrap (most easily appreciated in Figure 2a and c), and occasionally in spaces between layers of compact myelin (Figure 2a–e). Next, we examined the CNS of adult $Cnp^{+/Cre}$ mice harbouring the same td-tomato reporter construct, using epi-fluorescence microscopy. We observed td-tomato positive cell bodies, processes and myelin sheaths in all CNS areas examined,

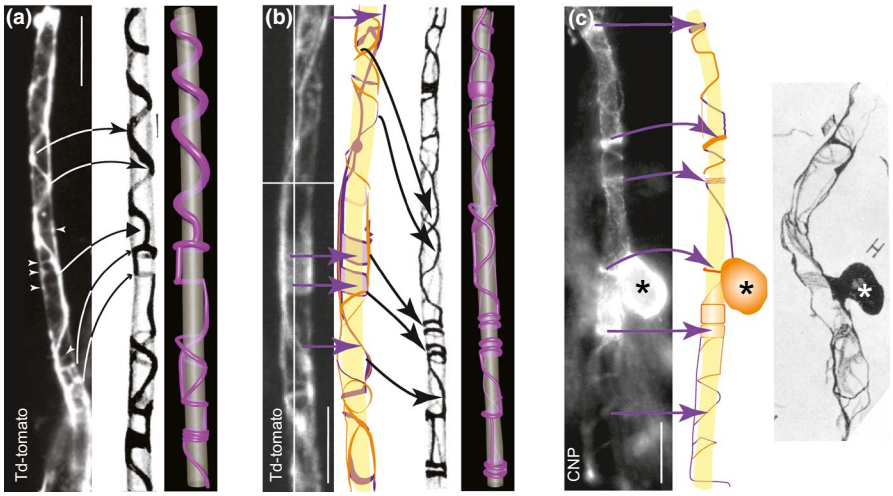

FIGURE 3 Td-tomato fluorescent protein and anti-CNP labelling illuminate the myelinic channel system in a manner resembling the drawings of Río-Hortega. (a) Live image taken using a widefield epi-fluorescence microscope of a td-tomato rendered sheath (the entire cell can be seen in Figure 4). Features similar to these in Figure 55E from Río-Hortega (1928), including spiralling coils with bell-shaped peaks (thin arrow heads), flat peaks (thick arrowhead) and *rings* or *bangles* (small arrow heads) are indicated. White arrowheads draw attention to faint labelling. Our 3D model of Río-Hortega's drawing is shown alongside (see also Supplementary movie 3A). (b) Maximum intensity projection (MIP) of a confocal z-stack of a td-tomato-rendered sheath of a live cell, taken using a spinning disc confocal microscope (see also Supplementary movie 3B of the z-stack), alongside a drawing made from the individual z-plane images (purple behind; orange in front; the axon in yellow has been extrapolated from the myelinic channel data), reminiscent of Figure 55B from Río-Hortega (1928), alongside our 3D model. Purple arrows indicate features of the fluorescence micrograph reproduced in the digital drawing. Black arrows indicate features similar to those seen in the drawing of Río-Hortega. (c) MIP of a z-stack of a CNP-stained cell taken using a widefield epi-fluorescence microscope, next to its trace made from the individual focal planes (purple behind; orange in front; extrapolated axon in yellow), alongside Figure 50H from Río-Hortega (1928) showing his 'monopolar' Schwannoid type 4 cell. The location of the CNP-stained cell body (asterisks) with respect to the sheath, and the presence of both thick and thin bands of cytoplasm appear similar to those features in Río-Hortega's drawing. Bars: 10 μm

including the spinal cord white matter (Figure 2f). Finally, we demonstrated in a murine spinal cord-derived myelinating cell culture system from the PLPCreERT2::floxed stop td-tomato transgenic line, that td-tomato fluorescent protein illuminates myelin sheaths (Figure 2g) whose termini colocalise with Caspr1, an axonal marker of paranodes (Figure 2h; Supplementary Figure 2). High resolution confocal imaging and super resolution imaging confirmed that td-tomato illuminated spiralling coils of cytoplasm (see schematic in inset) as would be expected at the paranodes, where paranodal loops entwine the axon (Figure 2i,j; Supplementary movies 2I and 2J 1 and 2). Td-tomato rendered sheaths stained with antibody to myelin basic protein (MBP; Figure 2j) and the presence of compact myelin was confirmed by electron microscopy (Figure 2k), as shown previously in this model (see Figures 3 and 4 in Thomson et al., (2008); Thomson et al., (2006), respectively). Thereafter, due to ease of visualisation, we used this cell culture model to examine the cytoplasmic channels of myelin for comparison with the drawings of Río-Hortega.

3.3 | Soluble fluorescent protein renders myelin cytoplasm as illustrated by Río-Hortega

The localisation of td-tomato in myelinating sheaths reminded us of the drawings of Río-Hortega (1928), so we compared side-by-side our own microscopic images with Río-Hortega's drawings (Figure 3a,b; Supplementary movies 3A and B). Given the role for CNP in keeping cytoplasmic channels open (Snaidero et al., 2017), we also examined the sheath location of CNP in relation to the drawings of Río-Hortega (Figure 3c). We found that both td-tomato and CNP illuminated features similar to those reported by Río-Hortega, including the rings, bangles, plates and 'bell-shaped' or 'flat-peaked' spiralling coils described above. We use the term *bangles* in Figure 3 legend to designate what Rio-Hortega described as thick striated rings (Supplementary File 1); *Plates* defines features that do not necessarily surround the axon circumference and *rings* encircle the axon.

3.4 | Single oligodendrocytes can wrap axons of diverse diameter

Although Río-Hortega classified oligodendrocytes into four types according to axon size, he commented that there is continuity in the spectrum. Nonetheless, due to the difficulty in discerning the morphology of individual oligodendrocytes *in vivo* (particularly in white matter), this has been difficult to confirm. Waxman and Sims (1984) provided evidence from imaging cross sections of developing rat spinal cord fibres that some cells wrap axons of different diameters. However, the diameter varies along the axon's length, applying

some uncertainty to this method. Almeida et al. (2011) showed using whole cell imaging in zebrafish, in which axon size was experimentally manipulated, that the same cell can wrap axons of diverse diameters. Here, we found evidence in myelinating cell cultures and in the drawings of Río-Hortega that occasionally, individual oligodendrocytes wrap axons of diverse diameters also in the mammalian nervous system (Figure 4).

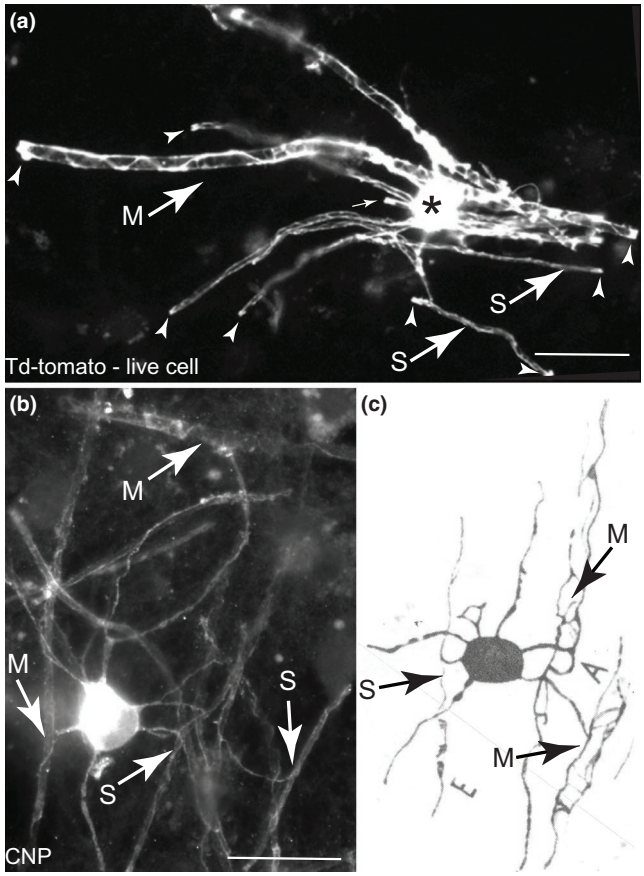

FIGURE 4 Individual oligodendrocytes can myelinate axons of diverse sizes. Micrographs taken using epi-fluorescence microscopes of (a) a live td-tomato illuminated oligodendrocyte and (b) a fixed, CNP stained oligodendrocyte, both *in vitro*. In both images, small (S) and medium (M) sized axons are myelinated by the same cell. Paranodal loops are indicated by small white arrows in a. (c) Figure 6E from Río-Hortega (1928) of dog white matter in which it appears the same cell body myelinates both small and medium diameter axons; excerpt from his Figure 6 where all three cells similarly myelinate both small and medium axons, based on his typical description of small axons with '*placular widening*' depicted near the letter *E*. Bars in a and b: 20 μm

3.5 | Mapping microtubules in myelinic channels

The myelinic channel system contains motile organelles (our unpublished observations) and mRNA for MBP, MOBP and others (Colman et al., 1982; Gould et al., 2000; Thakurela et al., 2016; Trapp et al., 1987), supporting its role as transport route. Microtubules populate the myelinic channel system as shown by the early electron microscopists (Figure 2 in Hirano & Dembitzer, 1967) and, when present, can be observed easily in inner and outer tongue processes and paranodal loops in well-preserved material (e.g. Figures 2 and 6 Hirano & Dembitzer, 1967; Figure 2 in Stassart et al., 2018, reproduced from Edgar & Griffiths, 2013). However, we inferred from often not observing microtubules in cytoplasmic spaces by EM (50–70 nm thick tissue sections; J. Edgar and W. Möbius, unpublished observations) that they are not continuous throughout the myelinic channel system. In myelinating cell cultures, oligodendrocyte-specific β-tubulin 4 antibody staining delineated paranodal loops (Figure 5a,b), bell-shaped and flat-peaked spiralling coils (Figure 5c–h), but not rings or bangles as observed with td-tomato or CNP staining. Furthermore, gaps were observed in β-tubulin 4 staining that were not seen with td-tomato (Figure 5b). Nonetheless, continuity in β-tubulin 4 staining between the process connecting to the cell body and the outer tongue is beyond doubt (Supplementary movies 5D, F and G). Together, these data suggest that in myelin, microtubule-dependent transport relies on dynamics of microtubules to surmount breaches in the transport highway.

3.6 | The myelinic channel system is not static

Myelin sheaths turn over their lipid and protein components and change length and thickness in response to neuronal activity (see Introduction). We speculate that the myelinic channel system, including its microtubule content, provides an infrastructure for this dynamic behaviour by facilitating active transport of materials for

FIGURE 5 β tubulin 4 delineates part of the myelinic channel system. (a) Maximum intensity projection of a confocal z-stack of β tubulin 4 (magenta), which can be observed along the td-tomato (white) illuminated internode, and at the paranodal loops marked by axonal Caspr1 (green). The white arrow points to the node of Ranvier. The inset shows consecutive 0.32 μm z-steps through the paranode on the right of the node of Ranvier, showing td-tomato and β tubulin 4. (b) β tubulin 4 is not continuous within the td-tomato-rendered space. In the upper image, a maximum intensity projection is shown of consecutive 0.32 μm z-step confocal images and in the lower image, a single z plane is shown, in which regions of td-tomato labelling are not stained by β tubulin 4 (small arrows). The large arrow points to a node of Ranvier. (c) Montage of the various focal planes of a z-stack taken using a widefield epi-fluorescence microscope of a cell stained with antibody to PLP/DM20 (white; a td-tomato positive cell, also in white, can be observed below the sheath) and β tubulin 4 (magenta). A digital drawing (upper left) outlines the tracing of in-focus magenta labelling through a series of focal planes from the z-stack. Small white arrows indicate a node of Ranvier between two paranodes. In the drawing, the axon (yellow) was extrapolated from the myelin data. (d) 3-D reconstruction of the digital drawing in (c). (e) Digital drawing as in (a) of a sheath from another cell. (f) The corresponding 3D reconstruction of (e). (g, h) Other sheaths of different cells in which β tubulin 4 delineated the cell process as well as bell-shaped spiralling coils, flat peaks, and paranodal loops. The axolemma, encompassing the axon cylinder, is depicted in grey, β tubulin 4 staining in blue. See also Supplementary movies 5D, F and G

synthesis or degradation. To determine if the myelinic channel system itself is dynamic, we used repetitive live imaging of mature myelin *in vitro* over short (15 minute) and longer (24–72 hour) intervals. Occasionally, we observed subtle changes over minute intervals (Figure 6a, DIV 28) or 24-hour intervals (Figure 6a–c), against a background of more general stability, as expected in established myelin sheaths. Specifically, structural features of the *myelinic channel system* and boluses of td-tomato translocated in the longitudinal direction (in relation to the sheath), over time. Whether there was also rotation or movement in the transverse direction is harder to conclude because (i) it was not possible to capture exactly the same focal planes in the z-direction on consecutive days and (ii) putative rotations could stem from twisting of the entire nerve fibre. Together, these results indicate that in the mature sheath, the

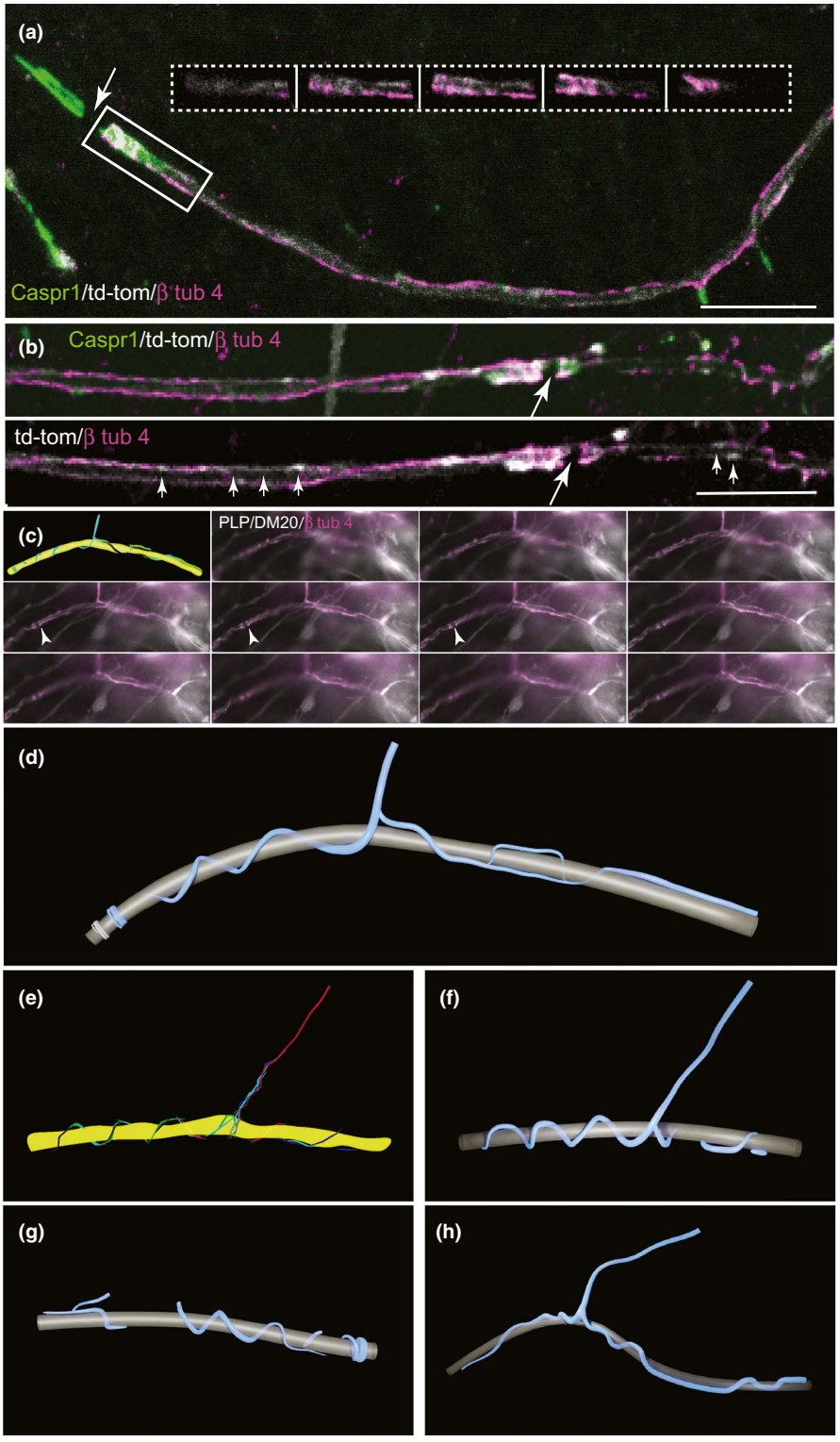

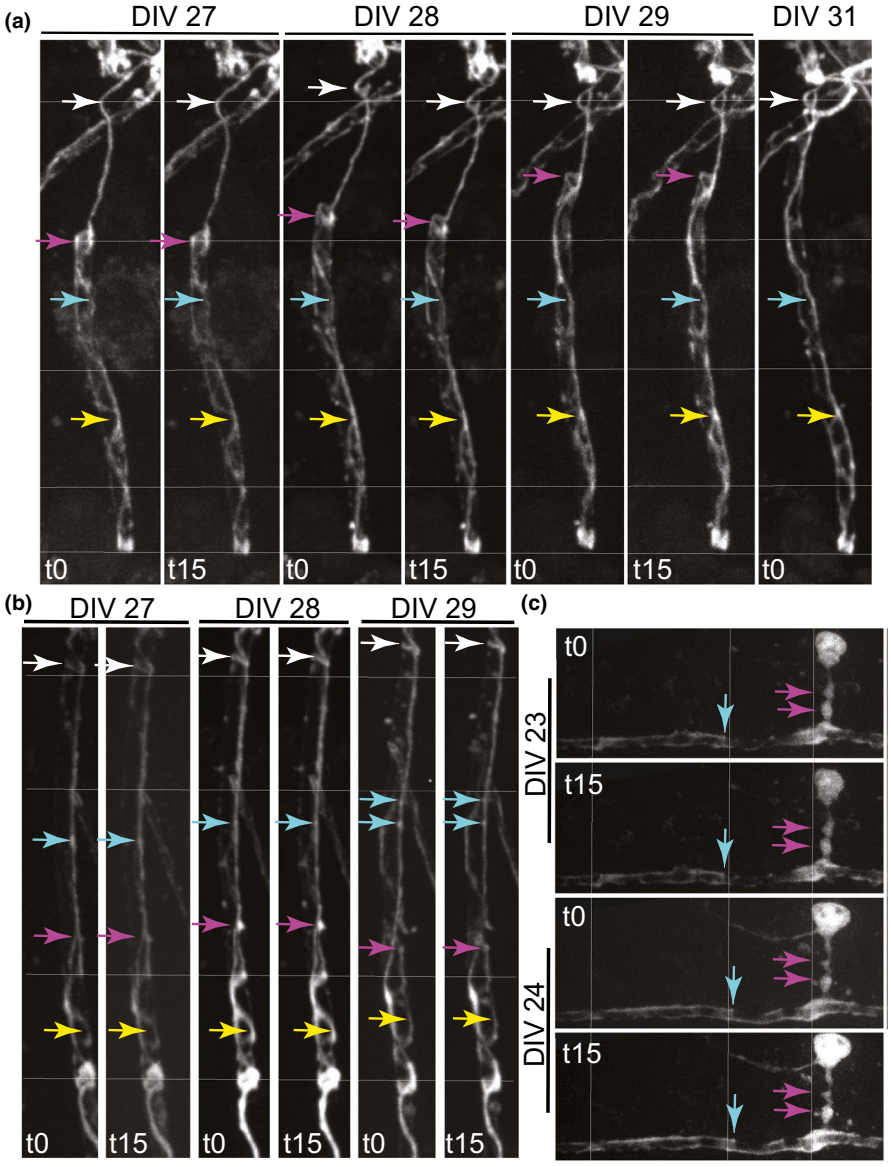

FIGURE 6 The established myelinic channel system is largely stable but can undergo subtle shape changes over time. (a–c) Maximum intensity projections of confocal z-stack live images of td-tomato illuminated myelin sheaths and in (c), the cell body also, over minutes or days. Cells were imaged each day at t0 and t15 min to assess acute changes and 24 or 48 h later to assess slower dynamic changes. Thin white lines mark specific distances in the vertical (a, b) and horizontal (c) axes across all the cells. Coloured arrows mark a specific feature over the various time points to highlight whether its location or shape changes. In (a), an acute change in location can be observed between t0 and t15 at DIV28 (upper white arrow), while a slower change in shape and location can be observed over days (magenta arrow). In (b), subtle changes in location can be observed at the white and magenta arrows. In (c), imaged at DIV 23 and 24, when the sheath is probably still wrapping, a subtle change in shape and location can be seen at the cyan arrow. A thick process from the cell body joins the sheath at right angles. This process reminds us of a 'corkscrew' with respect to its shape; a shape that is not unusual in our experience of live imaging of myelinating oligodendrocytes (see also Figure 3C and D in Butt & Ransom, 1989). t0 and t15 min images were taken in exactly the same z-stack at <0.5 μm intervals, whereas this was not possible across days, so we cannot exclude that some subtle 'changes' reflect that slightly different focal planes were imaged

myelinic channel system and its contents are not static, in line with current reports on the dynamics of myelin.

4 | DISCUSSION

Using expression of fluorescent protein in oligodendrocytes, we previously proposed a model in which the outer tongue process of myelin spirals around the axon in a corkscrew-like fashion (see Figure 5Ji and ii in Ioannidou et al., 2012). Here, we focus on the entire myelinic channel system, including spaces that we show by immunoelectron microscopy are located between layers of compact myelin. In fact, the myelinic channel system, although not conceptualised as such in the respective publications, is visible throughout the recent literature by virtue of expression of fluorescent 'reporter' proteins and immunostaining. For example,

in zebrafish myelin illuminated with soluble GFP (Almeida et al., 2011) or in human myelin following CNP staining of iPSC-derived myelinoids (see Figure 2B in James et al., 2021). These data demonstrate that the drawings of Río Hortega, despite his own doubts, are not artefactual.

The channel architecture we observe in mature sheaths is consistent with the current model of myelinogenesis, involving simultaneous spiral wrapping around the axon by growth at the inner tongue and lateral extension along the axon (Snaidero et al., 2014). However, our observation that in the established sheath, the β-tubulin 4 stained outer tongue spirals around the axon (our Figure 5, and see also Figures 8 Berry et al., 1995 and 5 Ioannidou et al., 2012) seems not entirely consistent with the long-established rectangular-shaped 'unrolled' model first proposed by Hirano and Dembitzer (1967). This leads us to propose a working model in which a fan-shaped outer-most aspect of the 'unrolled' sheath informs the shape at the inner aspect; this to generate a sheath of equal thickness along the internode (Figure 7). We further suggest the rings, bangles and plates in the mature sheath (see particularly our Figure 3) are generated by secondary growth involving reversal of direction of extension of cytoplasm-filled membrane at the zones of growth (Figure 7). Future work combined with advanced imaging methodologies will be required to finally resolve these issues, as well as those of function and implications for insulation.

Our interest in the cytoplasmic channels of myelin arose following three key observations. The first, that in mice lacking CNP due to gene inactivation (Lappe-Siefke et al., 2003), secondary axon changes and degeneration are associated with varicosity of the inner tongue process of oligodendrocytes (Edgar et al., 2009; Lappe-Siefke et al., 2003). The second being the observation that oligodendrocytes supply energy-rich metabolites to axons (Fünfschilling et al., 2012; Lee et al., 2012), presumably reaching the axon by way of the myelinic channel system (Saab et al., 2013). Indeed, the recent observation that CNP contributes to keeping the cytoplasmic channels of myelin open (Snaidero et al., 2017) raises the possibility that secondary axon degeneration (and inner tongue swelling) in the *Cnp1* knockout mouse reflects collapse of the myelinic channel system and impaired trafficking of glial-derived materials such as monocarboxylate transporters (Jha & Morrison, 2020; Lee et al., 2012) and metabolites to the glial–axonal junction, as speculated (Edgar et al., 2009; Nave, 2010). Finally, the adaxonal cytoplasmic compartment of the myelin sheath also contributes to the electric currents during saltatory impulse conduction (Cohen et al., 2020).

Río-Hortega was the first to succeed in visualising the cytoplasm of myelin in exquisite detail with his silver carbonate stain, but his method was rather capricious (Río-Hortega, 1928). It took the advent of soluble fluorescent reporter proteins to visualise the channel system again in its entirety. At 54 kDa, td-tomato (Shaner et al., 2004) is unlikely to pass through gap junctions and must reach its target by diffusion through open spaces. While not superior to Río-Hortega's silver stain in terms of resolution, fluorescent proteins, especially those whose expression can be switched on once the sheath is formed (as in this study), possess the advantage that we can infer that the regions in which they localise were in continuity with the cell body at the time of induction.

It is intriguing that a fluorescent protein renders eerily similar images to those drawn by Río-Hortega. Two observations come to mind. First, there appears to be minimal shrinkage with Río-Hortega's silver carbonate staining when compared with live labelling with fluorescent cytoplasmic tracers, suggesting that the cytoplasmic channels of myelin are densely filled with proteins. Second, one deliberates on the exact localisation of the complex web of channels (*rings*, *bangles*, *plates* and other confirmations) that we could not fully elucidate even with super-resolution imaging. Are these truly perimyelinic at the outer tongue level, as Río-Hortega (1928) believed the *cytoplasmic reticulum* to lie, or deeper in the sheath? Although the inner and outer tongues and paranodal loops of myelin are well known, the question arises why pockets of cytoplasm in compact myelin have largely been overlooked until recently. In the 1960s, open spaces between layers of compact myelin similar to those in our Figure 2 were reported in EM studies. For example, Bunge et al. (1961; see their schematic) described '*trapped cytoplasm*', while Hirano and Dembitzer (1967; see their Figure 3), and Peters et al. (1970) noticed '*isolated islands of cytoplasm*', whilst Hildebrand et al., (1993; see their Figure 19g) noted '*possibly cytoplasmic remnants*'. This, despite that EM in these early days, with a documented 10–30% myelin shrinkage, likely underrepresented the myelinic cytoplasmic channels (Kirschner & Hollingshead, 1980). Nonetheless, these open spaces in compact myelin were generally considered technical artefact for some time thereafter. Here we provide proof using immunoelectron microscopy, which avoids use of osmium thus decreasing the problem of shrinkage and better preserving the tissue's native structure, that in addition to inner and outer tongues and paranodal loops, td-tomato reached the (uncompacted) first wrap of myelin and spaces within compact myelin itself (Figure 2), confirming these are cytoplasm filled.

Importantly, images of CNP staining in a recent report describing the generation of iPSC-derived myelinoids confirms the existence of the myelinic channel system in human myelin (see Figure 2B in James et al., 2021). Moreover, the authors show anti-Claudin-11 immunostaining that is consistent with tight junctions lining the outer tongue and paranodal loops, at least in the vicinity of the node (see Figure 3 in James et al., 2021), as reported previously (Devaux et al., 2010; Schnapp & Mugnaini, 1976). Claudin-11 tight junctions also contributes to the lattice-shaped supramolecular structure of the radial component that traverses myelin lamellae (see Figure 8 in Kosaras & Kirschner, 1990), often between inner and outer tongues (Peters, 1964), providing strong mechanical coupling between adjacent myelin layers and acting in the maintenance of the sheath's insulative properties (Denninger et al., 2015).

Notwithstanding that adjacent layers of compact myelin are tightly packed, two studies (Snaidero et al., 2014; Velumian et al., 2011) showed that cytoplasmic spaces within compact myelin can open and close; coming 40 years after it was shown that PNS Schmidt-Lanterman incisures can dilate and constrict under experimental conditions (Hall & Williams, 1970). Using live imaging, we

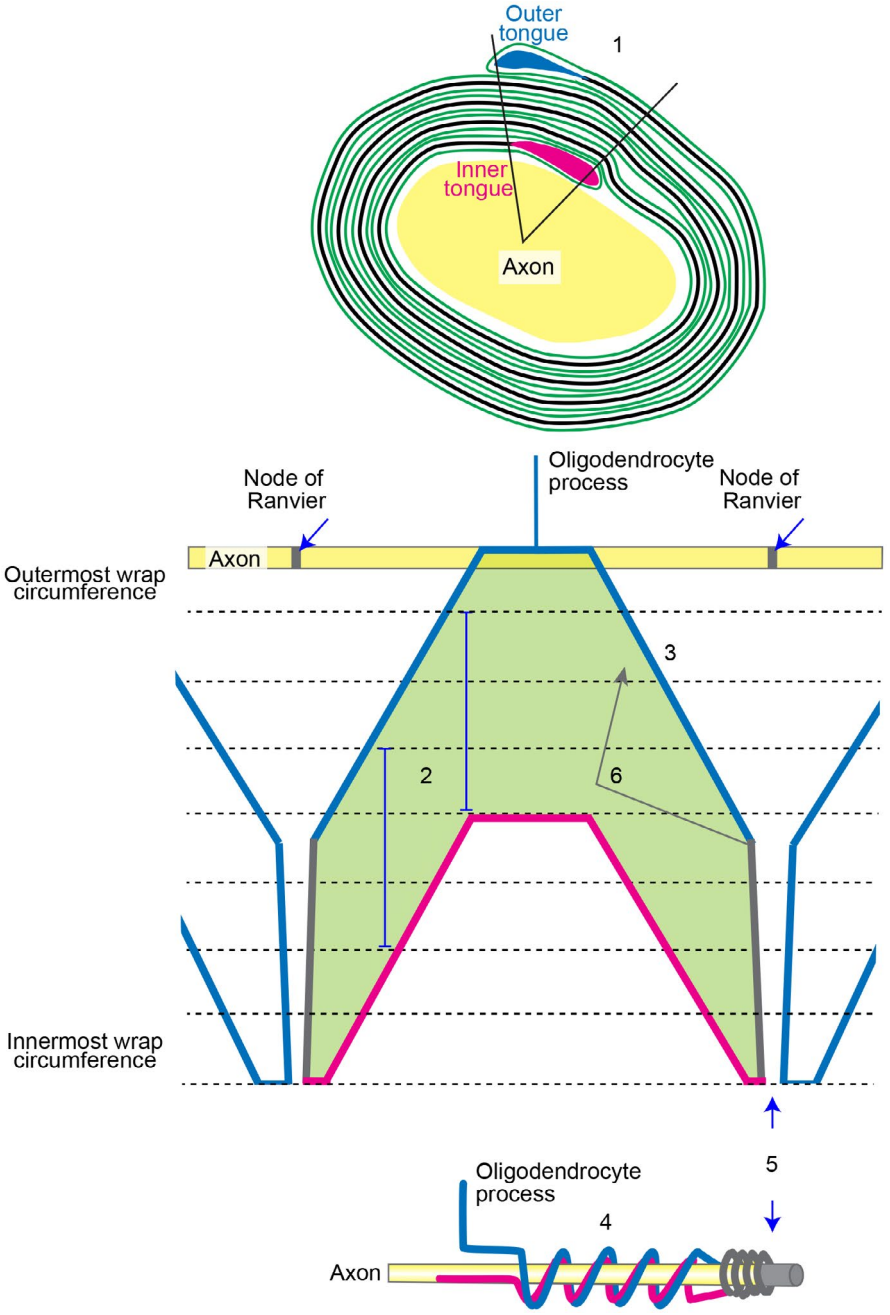

FIGURE 7 Working model of the unwrapped myelin sheath. 1. Outer and inner tongues are located in the same quadrant in ~75% of fibres viewed in cross section (Peters, 1964). 2. The sheath (green; the shape shown here is simplified for clarity) extends only by growth at the inner tongue (Snaidero et al., 2014; magenta). Vertical blue lines indicate the distance the lamellipod has extended between the position where it first contacted the sheath (uppermost part) and the position where extension at the glial–axonal junction ceases (lowermost part). This distance is constant along the internode. 3. The lamellipod shape as it extends away from the oligodendrocyte process is fan-shaped because the extreme leading edge (alone; eventually forming the inner tongue) drives protrusion forward and laterally from the point it hits the axon. 4. This fan shape gives rise to the corkscrew-like spiralling (bell-shaped and flat peaks) of the outer tongue as shown in our Figure 5. Thickening of the developing sheath proceeds (usually) from the middle of the internode (Figure 1 in Snaidero et al., 2014), but importantly, the mature sheath is equally thick along its length, thus the fan-shaped outer aspect informs the shape of the inner aspect. (Not shown in the diagram—the lamellipod's shape is stochastic due to variation in the environment and random collisions; the distance extended must therefore be informed by the location of the outer tongue (blue) to achieve equal thickness along the internode). 5. The fan shape ends at the presumptive node, where the leading edge (growth zone) fails to spread any further laterally. The paranodal loops (grey) abut the node. 6. Secondary reverse growth from the growth zone, separate from the lamellipod and located on the outside of sheath, could contribute to the *rings*, *bangles*, *plates* and other conformations described by Río Hortega, and noted in the current work

demonstrated that the myelinic channel system in its entirety does not change much over short time periods (here, 2–3 days), but bolus areas of fluorescent intensity and some morphological features translocated slowly over time (Figure 6), in line with recent reports suggesting myelin is less static than previously thought.

Finally, despite Río-Hortega's intricate drawings of cytoplasm associated with myelin, he is best known for defining oligodendrocytes into types depending upon the diameter of the axons they myelinate. However, Río-Hortega's own comments on a '*continuous spectrum*' has been described by others who note '*a morphological continuum*, and *transitional forms* [between types I/II and types III/IV]' (reviewed in Butt, 2013). These transitional forms have been convincingly reported *in vivo* (using images of entire sheaths) in rat (Berry et al., 1995) and, following experimental manipulation, in zebrafish (Almeida et al., 2011). The capacity of the same cell to wrap axons of diverse diameter is intriguing given that myelin sheath length, which correlates with axon diameter, is largely an intrinsic property of oligodendrocytes (Bechler et al., 2015). This suggests that there is also local regulation of sheath dimensions, at the level of the individual internode, emphasising once more, the remarkable morphological and functional complexity of Río-Hortega's '*oligodendroglia*'.

5 | SUMMARY AND PERSPECTIVE

In summary, we highlight some of Río-Hortega's lesser-known contributions to our understanding of oligodendroglia, including his intricate depictions of cytoplasm associated with myelin. Furthermore, we confirm the presence and complexity of the myelinic channel system which exhibits a degree of motility, supporting recent reports suggesting that myelin is far less static than previously thought. Our observations contribute to the ongoing revisions of our understanding of myelin architecture and function.

ACKNOWLEDGEMENTS

Pio del Río-Hortega's figures were reproduced with the kind permission of his grand-nephew, Juan del Río-Hortega Bereciartu. We are grateful to Mikael Simons for discussion and for critically reviewing the manuscript; to Professors Ueli Suter and Pierre Chambon, and Dr Daniel Metzger for gift of the PLP-Cre-ERT2 mice; to Professor Hongkui Zeng for the td-tomato (line Ai14) mice; to Professors Elior Peles and Nigel Groome for antibodies; Mailis McCulloch for EM of cell cultures and to our funders, the UK MS Society (Grant refs 38 and 127 to JE), NIH/National Library of Medicine (grant G13LM011465 to AB), the Deutsche Forschungsgemeinschaft (DFG, German Research Foundation) TRR 274/1 2020—408885537 to KAN), Research Center Nanoscale Microscopy and Molecular Physiology of the Brain, CNMPB (to KAN and WM) as well as the European Research Council (ERC, erc.europa.eu: ERC Advanced Grants AxoGlia and MyeliNANO to KAN).

CONFLICT OF INTEREST

The authors declare that they have no conflicts of interest.

AUTHOR CONTRIBUTIONS

AB, JME, KAN contributed to concept/design. JME, KJC, WM, LL acquired data. JME, AB, KAN analysed and interpreted data. EM generated 3D models: JME and RHI contributed to conception and illustration of unrolled model. JME, AB drafted the manuscript. JME, AB, KAN critically revised the manuscript. All authors approved and edited the article.

DATA AVAILABILITY STATEMENT

The raw data that support the findings of this study are available from the corresponding authors upon reasonable request.

ORCID

Julia M. Edgar https://orcid.org/0000-0002-3869-0962
Anne Boullerne https://orcid.org/0000-0001-5364-1088

REFERENCES

Aggarwal, S., Yurlova, L., Snaidero, N., Reetz, C., Frey, S., Zimmermann, J. et al. (2011) A size barrier limits protein diffusion at the cell surface to generate lipid-rich myelin-membrane sheets. *Developmental Cell*, 21, 445–456.

Almeida, R.G., Czopka, T., Ffrench-Constant, C. & Lyons, D.A. (2011) Individual axons regulate the myelinating potential of single oligodendrocytes in vivo. *Development*, 138, 4443–4450.

Arancibia-Cárcamo, I.L., Ford, M.C., Cossell, L., Ishida, K., Tohyama, K. & Attwell, D. (2017) Node of Ranvier length as a potential regulator of myelinated axon conduction speed. *Elife*, 6, e23329.

Bechler, M.E., Byrne, L. & Ffrench-Constant, C. (2015) CNS myelin sheath lengths are an intrinsic property of oligodendrocytes. *Current Biology*, 25, 2411–2416.

Bechler, M.E., Swire, M. & Ffrench-Constant, C. (2018) Intrinsic and adaptive myelination-A sequential mechanism for smart wiring in the brain. *Developmental Neurobiology*, 78, 68–79.

Berry, M., Ibrahim, M., Carlile, J., Ruge, F., Duncan, A. & Butt, A.M. (1995) Axon-glial relationships in the anterior medullary velum of the adult rat. *Journal of Neurocytology*, 24, 965–983.

Bijland, S., Thomson, G., Euston, M., Michail, K., Thümmler, K., Mücklisch, S. et al. (2019) An in vitro model for studying CNS white matter: functional properties and experimental approaches. *F1000Research*, 8, 117.

Blakemore, W.F. (1969) Schmidt-Lantermann incisures in the central nervous system. *Journal of Ultrastructure Research*, 29, 496–498.

Boullerne, A.I. (2016) The history of myelin. *Experimental Neurology*, 283, 431–445.

Brockschnieder, D., Sabanay, H., Riethmacher, D. & Peles, E. (2006) Ermin, a myelinating oligodendrocyte-specific protein that regulates cell morphology. *Journal of Neuroscience*, 26, 757–762.

Bunge, M.B., Bunge, R.P. & Ris, H. (1961) Ultrastructural study of remyelination in an experimental lesion in adult cat spinal cord. *The Journal of Biophysical and Biochemical Cytology*, 10, 67–94.

Bunge, R.P. (1968) Glial cells and the central myelin sheath. *Physiological Reviews*, 48, 197–251.

Buser, A.M., Erne, B., Werner, H.B., Nave, K.A. & Schaeren-Wiemers, N. (2009) The septin cytoskeleton in myelinating glia. *Molecular and Cellular Neurosciences*, 40, 156–166.

Butt, A.M. (2013) Structure and function of oligodendrocytes. In: Kettenmann, H. & Ransom, B. (Eds.) *Neuroglia*, 3rd edition. New York: Oxford University Press, pp. 62–85.

Butt, A.M. & Ransom, B.R. (1989) Visualization of oligodendrocytes and astrocytes in the intact rat optic nerve by intracellular injection of lucifer yellow and horseradish peroxidase. *Glia*, 2, 470–475.

Cajal, S.R.y. (1909–1911) *Histologie du Système Nerveux de l'Homme et des Vertébrés*. Paris: Maloine.

Cajal, S.R.y. (1913) Contribución al conocimiento de la neuroglia del cerebro humano. *Trabajos Del Laboratorio De Investigaciones Biológicas De La Universidad De Madrid*, 11, 255–315.

Cohen, C.C.H., Popovic, M.A., Klooster, J., Weil, M.-T., Möbius, W., Nave, K.-A. et al. (2020) Saltatory conduction along myelinated axons involves a periaxonal nanocircuit. *Cell*, 180, 311–322.e15.

Colman, D.R., Kreibich, G., Frey, A.B. & Sabatini, D.D. (1982) Synthesis and incorporation of myelin polypeptides into CNS myelin. *Journal of Cell Biology*, 95, 598–608.

De Robertis, E., Gerschenfeld, H.M. & Wald, F. (1958) Cellular mechanism of myelination in the central nervous system. *The Journal of Biophysical and Biochemical Cytology*, 4, 651–656.

Denninger, A.R., Breglio, A., Maheras, K.J., LeDuc, G., Cristiglio, V., Demé, B. et al. (2015) Claudin-11 tight junctions in myelin are a barrier to diffusion and lack strong adhesive properties. *Biophysical Journal*, 109, 1387–1397.

Devaux, J., Fykkolodziej, B. & Gow, A. (2010) Claudin proteins and neuronal function. *Current Topics in Membranes*, 65, 229–253.

Dutta, D.J., Woo, D.H., Lee, P.R., Pajevic, S., Bukalo, O., Huffman, W.C. et al. (2018) Regulation of myelin structure and conduction velocity by perinodal astrocytes. *Proceedings of the National Academy of Sciences of the United States of America*, 115, 11832–11837.

Edgar, J.M. & Griffiths, I.R. (2013) White matter structure: a microscopist's view. In: Johansen-Berg, H. & Behrens, T.E.J. (Eds.) *Diffusion MRI*. London: Elsevier, p. 127–149.

Edgar, J.M., McLaughlin, M., Werner, H.B., McCulloch, M.C., Barrie, J.A., Brown, A. et al. (2009) Early ultrastructural defects of axons and axon-glia junctions in mice lacking expression of Cnp1. *Glia*, 57, 1815–1824.

Edgar, J.M., Smith, R.S. & Duncan, I.D. (2020) Transmission electron microscopy and morphometry of the CNS white matter. *Methods in Molecular Biology*, 2143, 233–261.

Fünfschilling, U., Supplie, L.M., Mahad, D., Boretius, S., Saab, A.S., Edgar, J. et al. (2012) Glycolytic oligodendrocytes maintain myelin and long-term axonal integrity. *Nature*, 485, 517–521.

Ghabriel, M.N. & Allt, G. (1981) Incisures of Schmidt-Lanterman. *Progress in Neurobiology*, 17, 25–58.

Gould, R.M., Freund, C.M., Palmer, F. & Feinstein, D.L. (2000) Messenger RNAs located in myelin sheath assembly sites. *Journal of Neurochemistry*, 75, 1834–1844.

Hall, S.M. & Williams, P.L. (1970) Studies on the "incisures" of Schmidt and Lanterman. *Journal of Cell Science*, 6, 767–791.

Hildebrand, C., Remahl, S., Persson, H. & Bjartmar, C. (1993) Myelinated nerve fibres in the CNS. *Progress in Neurobiology*, 40, 319–384.

Hirano, A. & Dembitzer, H.M. (1967) A structural analysis of the myelin sheath in the central nervous system. *Journal of Cell Biology*, 34, 555–567.

Ioannidou, K., Anderson, K.I., Strachan, D., Edgar, J.M. & Barnett, S.C. (2012) Time-lapse imaging of the dynamics of CNS glial-axonal interactions in vitro and ex vivo. *PLoS One*, 7, e30775.

James, O.G., Selvaraj, B.T., Magnani, D., Burr, K., Connick, P., Barton, S.K. et al. (2021) iPSC-derived myelinoids to study myelin biology of humans. *Developmental Cell*, 56, 1346–1358.e6.

Jha, M.K. & Morrison, B.M. (2020) Lactate transporters mediate glia-neuron metabolic crosstalk in homeostasis and disease. *Frontiers in Cellular Neuroscience*, 14, 589582.

Karlsson, U. & Schultz, R.L. (1965) Fixation of the central nervous system from electron microscopy by aldehyde perfusion. i. preservation with aldehyde perfusates versus direct perfusion with osmium tetroxide with special reference to membranes and the extracellular space. *Journal of Ultrastructure Research*, 12, 160–186.

Kirschner, D.A. & Hollingshead, C.J. (1980) Processing for electron microscopy alters membrane structure and packing in myelin. *Journal of Ultrastructure Research*, 73, 211–232.

Knobler, R.L., Stempak, J.G. & Laurencin, M. (1976) Nonuniformity of the oligodendroglial ensheathment of axons during myelination in the developing rat central nervous system. A serial section electron microscopical study. *Journal of Ultrastructure Research*, 55, 417–432.

Kosaras, B. & Kirschner, D.A. (1990) Radial component of CNS myelin: junctional subunit structure and supramolecular assembly. *Journal of Neurocytology*, 19, 187–199.

Lappe-Siefke, C., Goebbels, S., Gravel, M., Nicksch, E., Lee, J., Braun, P.E. et al. (2003) Disruption of Cnp1 uncouples oligodendroglial functions in axonal support and myelination. *Nature Genetics*, 33, 366–374.

Lee, Y., Morrison, B.M., Li, Y., Lengacher, S., Farah, M.H., Hoffman, P.N. et al. (2012) Oligodendroglia metabolically support axons and contribute to neurodegeneration. *Nature*, 487, 443–448.

Leone, D.P., Genoud, S., Atanasoski, S., Grausenburger, R., Berger, P., Metzger, D. et al. (2003) Tamoxifen-inducible glia-specific Cre mice for somatic mutagenesis in oligodendrocytes and Schwann cells. *Molecular and Cellular Neurosciences*, 22, 430–440.

Lubetzki, C., Sol-Foulon, N. & Desmazières, A. (2020) Nodes of Ranvier during development and repair in the CNS. *Nature Reviews Neurology*, 16, 426–439.

Madisen, L., Zwingman, T.A., Sunkin, S.M., Oh, S.W., Zariwala, H.A., Gu, H. et al. (2010) A robust and high-throughput Cre reporting and characterization system for the whole mouse brain. *Nature Neuroscience*, 13, 133–140.

Meschkat, M., Steyer, A.M., Weil, M.-T., Kusch, K., Jahn, O., Piepkorn, L. et al. (2020) White matter integrity requires continuous myelin synthesis at the inner tongue. *BioRxiv*. https://doi.org/10.1101/2020.09.02.279612

Nave, K.-A. (2010) Myelination and the trophic support of long axons. *Nature Reviews Neuroscience*, 11, 275–283.

Patzig, J., Erwig, M.S., Tenzer, S., Kusch, K., Dibaj, P., Möbius, W. et al. (2016) Septin/anillin filaments scaffold central nervous system myelin to accelerate nerve conduction. *Elife*, 5, e17199.

Peters, A. (1960) The structure of myelin sheaths in the central nervous system of Xenopus laevis (Daudin). *The Journal of Biophysical and Biochemical Cytology*, 7, 121–126.

Peters, A. (1964) Further observations on the structure of myelin sheaths in the central nervous system. *Journal of Cell Biology*, 20, 281–296.

Peters, A., Palay, S., Webster, H.deF. (Eds.) (1970) *The Fine Structure of the Nervous System*, 1st edition. New York: Hoeber.

Rasband, M.N. & Peles, E. (2021) Mechanisms of node of Ranvier assembly. *Nature Reviews Neuroscience*, 22, 7–20.

Remahl, S. & Hildebrand, C. (1990) Relation between axons and oligodendroglial cells during initial myelination I. The glial unit. *Journal of Neurocytology*, 19, 313–328.

Río-Hortega, P.del. (1919) El "tercer elemento" de los centros nerviosos. I. La microgliá en estado normal. *Boletín de la Sociedad Española de Biología*, 9, 68–82. Translated in English in Sierra et al., 2016. The "Big-Bang" for modern glial biology: Translation and comments on Pío del Río-Hortega 1919 series of papers on microglia. Glia, 64(11):1801-1840.

Río-Hortega, P.del. (1921) Estudios sobre la neurología. La glía de escasas radiaciones (oligodendroglía). Boletín de la Real Sociedad Española de Historia Natural. *Boletín de la Real Sociedad Española de Historia Natural*, 21, 63–92. Translated in English by J.R. Iglesias-Rozas and M. Garrosa, 2012. Glia with very few processes (oligodendroglia) by Pío del Río-Hortega. Clinical Neuropathology, 31(6), pp. 440–459.

Río-Hortega, P.del. (1928) Tercera aportación al conocimiento morfológico e interpretación funcional de la oligodendroglía. *Memorias de la Real Sociedad Española de Historia Natural*, 14, 5–122. Translated in English in 2013 by J.R. Iglesias-Rozas and M. Garrosa with a biographical note: Pío del Río-Hortega's third contribution to

the morphological knowledge and functional interpretation of the oligodendroglia, Elsevier, London.
Saab, A.S., Tzvetanova, I.D. & Nave, K.-A. (2013) The role of myelin and oligodendrocytes in axonal energy metabolism. *Current Opinion in Neurobiology*, 23, 1065–1072.
Schnapp, B. & Mugnaini, E. (1976) Freeze-fracture properties of central myelin in the bullfrog. *Neuroscience*, 1, 459–467.
Shaner, N.C., Campbell, R.E., Steinbach, P.A., Giepmans, B.N.G., Palmer, A.E. & Tsien, R.Y. (2004) Improved monomeric red, orange and yellow fluorescent proteins derived from Discosoma sp. red fluorescent protein. *Nature Biotechnology*, 22, 1567–1572.
Snaidero, N., Möbius, W., Czopka, T., Hekking, L., Mathisen, C., Verkleij, D. et al. (2014) Myelin membrane wrapping of CNS axons by PI(3,4,5)P3-dependent polarized growth at the inner tongue. *Cell*, 156, 277–290.
Snaidero, N., Velte, C., Myllykoski, M., Raasakka, A., Ignatev, A., Werner, H.B. et al. (2017) Antagonistic functions of MBP and CNP establish cytosolic channels in CNS myelin. *Cell Reports*, 18, 314–323.
Stassart, R.M., Möbius, W., Nave, K.-A. & Edgar, J.M. (2018) The Axon-Myelin unit in development and degenerative disease. *Frontiers in Neuroscience*, 12, 467.
Stensaas, L.J. & Stensaas, S.S. (1968) Astrocytic neuroglial cells, oligodendrocytes and microgliacytes in the spinal cord of the toad. II. Electron microscopy. *Zeitschrift für Zellforschung und mikroskopische Anatomie*, 86, 184–213.
Thakurela, S., Garding, A., Jung, R.B., Müller, C., Goebbels, S., White, R. et al. (2016) The transcriptome of mouse central nervous system myelin. *Scientific Reports*, 6, 25828.
Thomson, C.E., Hunter, A.M., Griffiths, I.R., Edgar, J.M. & McCulloch, M.C. (2006) Murine spinal cord explants: a model for evaluating axonal growth and myelination in vitro. *Journal of Neuroscience Research*, 84, 1703–1715.
Thomson, C.E., McCulloch, M., Sorenson, A., Barnett, S.C., Seed, B.V., Griffiths, I.R. et al. (2008) Myelinated, synapsing cultures of murine spinal cord–validation as an in vitro model of the central nervous system. *European Journal of Neuroscience*, 28, 1518–1535.
Trapp, B.D., Bernier, L., Andrews, S.B. & Colman, D.R. (1988) Cellular and subcellular distribution of 2',3'-cyclic nucleotide 3'-phosphodiesterase and its mRNA in the rat central nervous system. *Journal of Neurochemistry*, 51, 859–868.
Trapp, B.D., Moench, T., Pulley, M., Barbosa, E., Tennekoon, G. & Griffin, J. (1987) Spatial segregation of mRNA encoding myelin-specific proteins. *Proceedings of the National Academy of Sciences of the United States of America*, 84, 7773–7777.
Velumian, A.A., Samoilova, M. & Fehlings, M.G. (2011) Visualization of cytoplasmic diffusion within living myelin sheaths of CNS white matter axons using microinjection of the fluorescent dye Lucifer Yellow. *NeuroImage*, 56, 27–34.
Waxman, S.G. & Sims, T.J. (1984) Specificity in central myelination: evidence for local regulation of myelin thickness. *Brain Research*, 292, 179–185.
Weber, P., Metzger, D. & Chambon, P. (2001) Temporally controlled targeted somatic mutagenesis in the mouse brain. *European Journal of Neuroscience*, 14, 1777–1783.
Weil, M.-T., Ruhwedel, T., Meschkat, M., Sadowski, B. & Möbius, W. (2019) Transmission electron microscopy of oligodendrocytes and myelin. *Methods in Molecular Biology*, 1936, 343–375.
Werner, H.B., Kuhlmann, K., Shen, S., Uecker, M., Schardt, A., Dimova, K. et al. (2007) Proteolipid protein is required for transport of sirtuin 2 into CNS myelin. *Journal of Neuroscience*, 27, 7717–7730.
Weruaga-Prieto, E., Eggli, P. & Celio, M.R. (1996) Topographic variations in rat brain oligodendrocyte morphology elucidated by injection of Lucifer Yellow in fixed tissue slices. *Journal of Neurocytology*, 25, 19–31.
Wu, C., Chang, A., Smith, M.C., Won, R., Yin, X., Staugaitis, S.M. et al. (2009) Beta4 tubulin identifies a primitive cell source for oligodendrocytes in the mammalian brain. *Journal of Neuroscience*, 29, 7649–7657.
Yang, S.M., Michel, K., Jokhi, V., Nedivi, E. & Arlotta, P. (2020) Neuron class-specific responses govern adaptive myelin remodeling in the neocortex. *Science*, 370.

SUPPORTING INFORMATION

Additional supporting information may be found in the online version of the article at the publisher's website.

How to cite this article: Edgar, J.M., McGowan, E., Chapple, K.J., Möbius, W., Lemgruber, L., Insall, R.H., et al (2021) Río-Hortega's drawings revisited with fluorescent protein defines a cytoplasm-filled channel system of CNS myelin. *Journal of Anatomy*, 239, 1241–1255. https://doi.org/10.1111/joa.13577